# Resonant electromagnetic emission from intrinsic Josephson-junction stacks with laterally modulated Josephson critical current

A. E. Koshelev
*Materials Science Division, Argonne National Laboratory, Argonne, Illinois 60439, USA*

L. N. Bulaevskii
*Los Alamos National Laboratory, Los Alamos, New Mexico 87545, USA*

(Received 5 September 2007; revised manuscript received 20 November 2007; published 30 January 2008)

Intrinsic Josephson-junction stacks realized in mesas fabricated out of high-temperature superconductors may be used as sources of coherent electromagnetic radiation in the terahertz range. The major challenge is to synchronize Josephson oscillations in all junctions in the stack to get significant radiation out of the crystal edge parallel to the $c$ axis. We suggest a simple way to solve this problem via artificially prepared lateral modulation of the Josephson critical current identical in all junctions. In such a stack, phase oscillations excite the in-phase Fiske mode when the Josephson frequency matches the Fiske-resonance frequency which is set by the stack lateral size. The powerful, almost standing electromagnetic wave is excited inside the crystal in the resonance. This wave is homogeneous across the layers, meaning that the oscillations are synchronized in all junctions in the stack. We evaluate behavior of the $I$-$V$ characteristics and radiated power near the resonance for arbitrary modulation and find exact solutions for several special cases corresponding to symmetric and asymmetric modulations of the critical current.

DOI: 10.1103/PhysRevB.77.014530 PACS number(s): 74.50.+r, 85.25.Cp, 74.81.Fa, 74.72.Hs

## I. INTRODUCTION

Josephson junctions are natural voltage-to-frequency converters, since a finite voltage drop across the junction always leads to oscillating current with frequency proportional to the voltage (ac Josephson effect[1]). This fundamental property suggested an attractive possibility to use the ac Josephson effect for developing voltage-tunable generators of electromagnetic waves. Radiation from a Josephson junction directly into the waveguide in the microwave frequency range has been indeed detected a long time ago.[2,3] However, the typical detected radiated power $\sim 1$ pW occurred to be too small for practical applications.

A natural route to enhance this power is to use large arrays of junctions. This possibility has been extensively explored by several experimental groups; see reviews.[4,5] When all junctions oscillate in phase, the total emitted power is expected to be proportional to the square of the total number of junctions in the array. Inevitable variations of junction parameters, however, may cause variations of the oscillating frequencies, leading to desynchronization and dramatic drop in emission power. Therefore, the major challenge is to synchronize oscillations in all junctions.[4] One way to solve this problem is to couple the junctions with a resonant cavity. The efficient synchronization in such systems has been demonstrated experimentally[6] and has been extensively studied in several simulation papers.[7,8]

Demonstration of intrinsic Josephson effect in high-temperature superconductors[9] opened a completely new route to developing electromagnetic sources. Layered high-temperature superconducting materials, such as $Bi_2Sr_2CaCu_2O_8$ (BSCCO), are composed of superconducting $CuO_2$ layers coupled by Josephson interaction. Intrinsic Josephson effect has been extensively investigated in the past decade and most "classical" ac and dc Josephson phenomena have been observed, including Fraunhofer magnetic oscillations of critical current in small-size samples,[10] Josephson plasma resonance,[11,12] Shapiro steps in current-voltage characteristics induced by external microwave irradiation,[13,14] Fiske resonances,[15–17] etc. Therefore, a small-size mesa fabricated out of this material represents a natural one-dimensional array of Josephson junctions. A large value of superconducting gap, up to 60 meV, permits to bring the Josephson frequency into the practically important terahertz range. Due to atomic nature of the intrinsic junctions, it is much easier to prepare large arrays of virtually identical junctions than in artificially fabricated arrays. Nevertheless, the same challenge to synchronize oscillations in all junctions also remains for this system.

Electromagnetic waves propagate inside large-size layered superconductor in the form of plasma modes. In zero magnetic field, the minimum frequency of these waves corresponding to homogeneous oscillations is given by the Josephson plasma frequency. The in-plane velocity of the mode strongly depends on the $c$-axis wave vector, $q_z$. The highest velocity corresponds to the in-phase mode, $q_z=0$, and the lowest velocity corresponds to the antiphase mode, $q_z=\pi/s$.

A stack of the intrinsic Josephson junctions with lateral size smaller than the decay length of electromagnetic wave behaves as a cavity. It is characterized by a spectrum of Fiske resonant modes corresponding to excitation of almost standing electromagnetic waves.[18] Frequencies of these modes strongly depend on the wave vector perpendicular to the layer direction, with the maximum frequency corresponding to the homogeneous in-phase mode in all junctions and the minimum frequency corresponding to the antiphase mode. At the stack edge, the electromagnetic waves excited inside the intrinsic junctions are converted into electromagnetic waves propagating into dielectric media outside the crystal. To use the stack as a coherent source of such radiation, it would be

 

desirable to excite the in-phase resonance mode. Then the radiation power is proportional to the square of the total number of junctions positioned at distances smaller than the wavelength of radiation. However, to synchronize the intrinsic junctions, one needs to have strong enough coupling between them. In the simplest case of a homogeneous stack at zero magnetic field, the Josephson oscillations typically interact very weakly inside the crystal.

A very popular way to achieve coherent Josephson oscillations in the whole stack is to apply magnetic field along the layers. The magnetic field promotes strong inductive interaction between the neighboring junctions. Large magnetic field generates a dense Josephson vortex (JV) lattice homogeneously filling all junctions. In the case of large-size system, interaction between the static JV arrays in neighboring junctions leads to formation of the triangular lattice corresponding to the $\pi$ phase shift between the phases in the neighboring junctions. The Fiske resonances excited by the moving JV lattice have been observed experimentally.[15–17] Due to its triangular ground state, the JV lattice typically excites the antiphase modes. Only a very weak outside radiation at double Josephson frequency is expected in this case.[19]

To achieve a powerful emission, it would be desirable to prepare aligned rectangular arrangement of JVs. Such configuration is expected at certain conditions in small-size mesas due to interaction with edges. At small lattice velocities, transition from triangular to rectangular configuration with increasing magnetic field has been observed experimentally as a crossover from $\Phi_0/2$- to $\Phi_0$-periodic magnetic oscillations of the flux-flow voltage.[20] The transitions between *static* configurations have been studied theoretically in Ref. 21. The possibility to have the aligned configuration at large velocities is an open issue. Recent large-scale numerical simulations[22] suggest that excitation of the resonance in-phase mode and interaction via the radiation electromagnetic field may promote alignment of JVs.

A possibility to use a mesa with small lateral size and a very large number of junctions (about $10^4$) in zero magnetic field as a source of terahertz radiation has been proposed in Ref. 23. In such a design, oscillations in different junctions are synchronized by the external electromagnetic radiation field generated by the oscillations themselves. Small lateral size increases the strength of interaction due to the radiation field and allows to avoid excessive heating. Such a source is frequency tunable, with the maximum power conversion efficiency about 30%. The obvious technological challenge of this design is a requirement to fabricate a mesa with such a large number of almost identical junctions.

In this paper, we explore a different way to excite resonance mode and synchronize oscillations in a junction stack. We propose to use a stack with strongly modulated Josephson critical current (JCC), with modulation identical in all junctions. Such a modulation dramatically enhances coupling between the Josephson oscillations and the in-phase resonance modes. For a single junction, such a mechanism of excitation of the Fiske resonances has been considered in Ref. 24.

The frequencies of in-phase resonance modes are set by the lateral size of the mesa, $L$,

$$\omega_m = \frac{c}{\sqrt{\varepsilon_c}} \frac{m\pi}{L}, \tag{1}$$

where $\varepsilon_c$ is the $c$-axis dielectric constant. In particular, assuming $\varepsilon_c = 12$, the resonance at $\omega_1/2\pi = 1$ THz for the fundamental mode, $m=1$, takes place for a mesa with width 43 $\mu$m. In the resonance, a powerful, almost standing wave is excited by Josephson oscillations, which synchronizes oscillations in the whole stack. Such synchronization function of the cavity mode does not exist in a single junction.[24] In such a design, the frequency tunability in a single device is sacrificed in favor of larger power and better efficiency. We consider several specific cases of modulation, both symmetric and asymmetric, which correspond to excitation of the mode with the wavelength equal to $L$ and $2L$. For simplicity, we assume that the mesa size along the field direction, $L_y$, is larger than the wavelength of outcoming electromagnetic wave, $\lambda_\omega$ (0.3 mm for 1 THz). The calculation can be straightforwardly generalized to the opposite case $L_y < \lambda_\omega$. We calculate the $I$-$V$ dependences, radiated electromagnetic power, and power conversion efficiency for such systems.

Recently, the resonant electromagnetic emission from the mesas fabricated out of underdoped BSCCO crystals has been detected experimentally.[25] The resonance frequencies vary from 0.4 to 0.85 THz, and they increase roughly inversely proportional to the mesa widths. The origin of the observed resonances is most probably due to the mechanism described in this paper, even though no JCC modulation has been introduced deliberately. Suppression of superconductivity near the edges during the fabrication process occurs to be sufficient for excitation of the resonances. One can expect that deliberately introduced JCC modulation will significantly enhance the amplitude of the resonance and radiation power.

The paper is organized as follows. In Sec. II, we present the equation and boundary conditions for the oscillating phase when it is identical in all junctions. Derivation of the boundary condition for this case is summarized in Appendix A. We also present the radiation power in terms of the oscillating phase and power conversion efficiency. In Sec. III, we derive the energy-balance relations in the dynamic state. In Sec. IV, using these relations, we analyze the behavior near the resonances and derive approximate results for resonant enhancements of the current, radiated power, and power conversion efficiency. Appendix B presents derivation of the radiation losses for the resonance mode in a thin rectangular mesa. In Sec. V, we consider several special cases of modulation for which the problem allows for exact analytical solutions (see Fig. 1). We perform a detailed analysis of transport and radiation properties for these cases.

## II. GENERAL RELATIONS

We consider a stack of intrinsic Josephson junctions (mesa) located at $0 < x < L$, with modulated JCC $j_J(x) = g(x) j_J$, where $j_J$ is the JCC density at the reference point at which $g(x)=1$. When all junctions oscillate in-phase, the $c$-axis homogeneous phase obeys the following reduced equation:

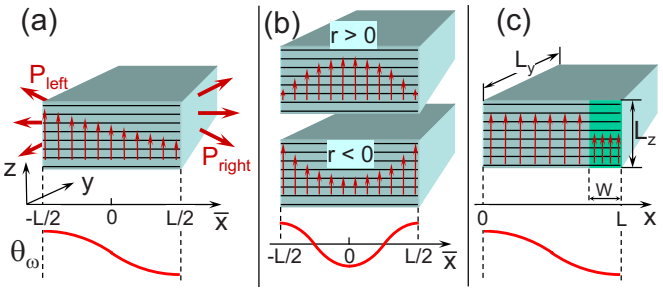


FIG. 1. (Color online) Mesas with modulation of the Josephson critical current density considered in the paper: (a) linear modulation, (b) parabolic modulation, and (c) steplike suppression of the critical current near the edge. The lower plots illustrate the shapes of lowest excited Fiske-resonance modes.

$$\frac{\partial^2\varphi}{\partial\tau^2}+\nu_c\frac{\partial\varphi}{\partial\tau}+g(x)\sin\varphi-\frac{\partial^2\varphi}{\partial x^2}=0, \tag{2}$$

in which the unit of length is the $c$-axis London penetration depth $\lambda_c$ and the unit of time is the inverse plasma frequency $1/\omega_p$. Both $\lambda_c$ and $\omega_p$ are also defined at the reference point at which $g(x)=1$. We will use these reduced units throughout the paper, converting to real units only in some important final results. The reduced damping parameter $\nu_c$ is related to the quasiparticle tunneling conductivity, $\nu_c=4\pi\sigma_c/\varepsilon_c\omega_p$. We will neglect inhomogeneity in the dissipation parameter $\nu_c$, because dissipation plays a minor role in the following consideration.

In the resistive state, the phase is given by

$$\varphi=\tilde{\omega}\tau+\theta(\tau,x),\quad \theta(\tau,x)=\mathrm{Re}[\theta_\omega(x)\exp(-i\tilde{\omega}\tau)], \tag{3}$$

where $\tilde{\omega}=\omega/\omega_p$ is the reduced Josephson frequency. We will use the linear approximation for the oscillating phase $\theta(\tau,x)$ valid for $\theta(\tau,x)<1$. As $\sin(\tilde{\omega}\tau)=\mathrm{Re}[i\exp(-i\tilde{\omega}\tau)]$, the amplitude of the oscillating phase, $\theta_\omega$, obeys the following equation:

$$(\tilde{\omega}^2+i\nu_c\tilde{\omega})\theta_\omega+\frac{\partial^2\theta_\omega}{\partial x^2}=ig(x). \tag{4}$$

The boundary conditions follow from the relation between the oscillating electric and magnetic fields in outside medium and the Josephson relations between the oscillating phase and these fields.[19] In general, the boundary conditions for the $c$-axis homogeneous oscillating phase describing radiation can be written as

$$\frac{\partial\theta}{\partial x}=\pm\int_{-\infty}^{\tau}d\tau'\beta(\tau-\tau')\frac{\partial\theta}{\partial\tau'}\quad\text{for } x=0 \text{ and } L \tag{5}$$

or, in Fourier representation,

$$\partial\theta_\omega/\partial x=\mp i\zeta\theta_\omega\quad\text{for } x=0 \text{ and } L \tag{6}$$

with

$$\zeta=\tilde{\omega}\beta_\omega\quad\text{and}\quad\beta_\omega=\int_0^\infty d\tau\beta(\tau)\exp(i\omega\tau).$$

Here, the kernel $\beta(\tau-\tau')$ depends on electromagnetic properties of the outside media. These boundary conditions assume that there is only outcoming waves at both boundaries. This means that we neglect reflected waves, coming back to the stack, and mixture of radiation coming from the opposite sides. Such a mixture can be suppressed if the mesa is bounded by large metallic contacts on both sides acting like screens. Derivation of the boundary condition in such a situation is presented in Appendix A and gives the following result for $\zeta(\tilde{\omega})$:

$$\zeta=\tilde{\omega}\beta_\omega=\frac{L_z\tilde{\omega}}{2\varepsilon_c\lambda_c}\left[|\tilde{\omega}|-\frac{2i\tilde{\omega}}{\pi}\ln\frac{5.03\sqrt{\varepsilon_c}\lambda_c}{|\tilde{\omega}|L_z}\right]. \tag{7}$$

The radiation losses are determined by the real part of $\zeta$. Its imaginary part only slightly displaces the resonance frequencies. In the following, we will neglect the imaginary part in the analytical estimates. Using typical values $N=1000$ and $\lambda_c=185\ \mu$m,[26] we estimate $sN/2\varepsilon_c\lambda_c=3.5\times10^{-4}$, indicating that $|\zeta|$ is typically very small.

The oscillating phase determines transport and radiation properties of the mesa. Without interference, the total radiation loss, $P_{\mathrm{tot}}$, is a sum of radiation powers coming from the left and right sides, $P_{\mathrm{tot}}(\omega)=P_{\mathrm{left}}(\omega)+P_{\mathrm{right}}(\omega)$. The left-side power, $P_{\mathrm{left}}$, is given by Poynting vector at the boundary, which is determined by the oscillating electric and magnetic fields at this side. These fields, in turn, may be related to the boundary value of the phase, $\theta_\omega(0)$. In the case of the boundary with free space, in real units, $P_{\mathrm{left}}(\omega)$ can be presented as[19]

$$P_{\mathrm{left}}(\omega)=L_y\frac{\Phi_0^2\omega^3N^2}{64\pi^3c^2}|\theta_\omega(0)|^2. \tag{8}$$

Correspondingly, the power radiated from the right side, $P_{\mathrm{right}}$, is obtained from this formula by replacement $\theta_\omega(0)\to\theta_\omega(L)$. For $\omega/2\pi=1$ THz and $N=1000$, we obtain an estimate for the prefactor,

$$\frac{\Phi_0^2\omega^3N^2}{64\pi^3c^2}\approx0.6\frac{\mathrm{W}}{\mathrm{cm}}.$$

This estimate provides the upper limit for possible radiation power in the case of strong resonance $\theta_\omega\sim1$.

We can also obtain a useful general expression for the power conversion efficiency, $Q=P_{\mathrm{tot}}/j_zE_zL$, the fraction of the total power fed to the junction which is converted to radiation. The total power fed into the stack can be represented as

$$j_zE_z=\frac{\Phi_0^2\omega}{s^2\pi(4\pi\lambda_c)^2}(\nu_c\tilde{\omega}+i_J), \tag{9}$$

where $\nu_c\tilde{\omega}$ is the quasiparticle current $\sigma_cE_z$ in units of $j_J$, and $i_J\equiv\langle g(x)\sin\phi\rangle$ is the reduced JCC density,

$$i_J \approx \frac{1}{2L}\int_0^L dx g(x)\mathrm{Re}[\theta_\omega(x)]. \tag{10}$$

Combining Eqs. (8) and (9), we derive

$$Q = \frac{\mathrm{Re}[\zeta]}{2L}\frac{|\theta_\omega(0)|^2 + |\theta_\omega(L)|^2}{\nu_c\tilde{\omega} + i_J}. \tag{11}$$

In the following sections, we will first consider the behavior near the resonance frequencies and then we will present the most interesting special cases of modulation allowing for exact solutions.

## III. ENERGY BALANCE

We consider first the energy-balance relations. The reduced energy in units of $L_z L_y \Phi_0^2/32\pi^3 s^2 \lambda_c$ accumulated in the phase oscillations inside the stack is given by

$$\mathcal{E} = \int_0^L dx\left[\frac{1}{2}\left(\frac{\partial\theta}{\partial\tau}\right)^2 + \frac{1}{2}\left(\frac{\partial\theta}{\partial x}\right)^2\right]. \tag{12}$$

Therefore, the energy-change rate is given by

$$\frac{\partial\mathcal{E}}{\partial\tau} = \int_0^L dx\frac{\partial\theta}{\partial\tau}\left[\frac{\partial^2\theta}{\partial\tau^2} - \frac{\partial^2\theta}{\partial x^2}\right] + \left[\frac{\partial\theta}{\partial\tau}\frac{\partial\theta}{\partial x}\right]_L - \left[\frac{\partial\theta}{\partial\tau}\frac{\partial\theta}{\partial x}\right]_0. \tag{13}$$

Following Eq. (2), the first term can be transformed to

$$\int_0^L dx\frac{\partial\theta}{\partial\tau}\left[\frac{\partial^2\theta}{\partial\tau^2} - \frac{\partial^2\theta}{\partial x^2}\right] = -\nu_c\int_0^L dx\left(\frac{\partial\theta}{\partial\tau}\right)^2 - \int_0^L dx\frac{\partial\theta}{\partial\tau}g(x)\sin\tilde{\omega}\tau.$$

Here, the first term accounts for the quasiparticle damping, while the second term gives the driving force from the Josephson oscillations leading to pumping of energy from a dc source into the electromagnetic oscillations inside the stack. The last two terms in Eq. (13) account for the radiation losses at the boundaries. For the general boundary conditions (5), these terms can be transformed as

$$\left[\frac{\partial\theta}{\partial\tau}\frac{\partial\theta}{\partial x}\right]_L - \left[\frac{\partial\theta}{\partial\tau}\frac{\partial\theta}{\partial x}\right]_0 = -\left[\frac{\partial\theta}{\partial\tau}\hat{\beta}\frac{\partial\theta}{\partial\tau}\right]_L - \left[\frac{\partial\theta}{\partial\tau}\hat{\beta}\frac{\partial\theta}{\partial\tau}\right]_0,$$

where we introduce a notation for the operator $\hat{\beta}\frac{\partial\theta}{\partial\tau} = \int_{-\infty}^{\tau} d\tau' \beta(\tau-\tau')\frac{\partial\theta}{\partial\tau'}$. Therefore, the total energy-change rate can be written as

$$\frac{\partial\mathcal{E}}{\partial\tau} = -\nu_c\int_0^L dx\left(\frac{\partial\theta}{\partial\tau}\right)^2 - \int_0^L dx\frac{\partial\theta}{\partial\tau}g(x)\sin(\tilde{\omega}\tau) - \left[\frac{\partial\theta}{\partial\tau}\hat{\beta}\frac{\partial\theta}{\partial\tau}\right]_L - \left[\frac{\partial\theta}{\partial\tau}\hat{\beta}\frac{\partial\theta}{\partial\tau}\right]_0. \tag{14}$$

For a steady state, the energy has to remain constant, meaning that the energy supplied by the Josephson oscillations has to be exactly compensated by the quasiparticle and radiation losses.

## IV. BEHAVIOR NEAR RESONANCES FOR ARBITRARY MODULATION

In this section, we obtain approximate results for the current and radiation in the vicinity of the resonance frequency $\tilde{\omega}_m = m\pi/L$, where the phase can be approximated as the corresponding cavity mode

$$\theta(x) \approx \psi\cos(m\pi x/L). \tag{15}$$

We neglect the small influence of the radiation on the shape of the resonance mode. In this case, the energy in the mode (12) and energy-change rate (14) can be approximated as

$$\mathcal{E} \approx \frac{L}{2}\left[\frac{1}{2}\left(\frac{\partial\psi}{\partial\tau}\right)^2 + \frac{1}{2}\tilde{\omega}_m^2\psi^2\right], \tag{16}$$

$$\frac{\partial\mathcal{E}}{\partial\tau} \approx -\frac{L}{2}\left[\nu_c\left(\frac{\partial\psi}{\partial\tau}\right)^2 + \frac{\partial\psi}{\partial\tau}g_m\sin\tilde{\omega}\tau + \frac{4}{L}\frac{\partial\psi}{\partial\tau}\hat{\beta}\frac{\partial\psi}{\partial\tau}\right], \tag{17}$$

where

$$g_m = \frac{2}{L}\int_0^L dx\cos\left(\frac{m\pi x}{L}\right)g(x) \tag{18}$$

is the coupling parameter. Therefore, equation for the mode amplitude is given by

$$\frac{\partial^2\psi}{\partial\tau^2} + \tilde{\omega}_m^2\psi + \nu_c\frac{\partial\psi}{\partial\tau} + \frac{4}{L}\hat{\beta}\frac{\partial\psi}{\partial\tau} = -g_m\sin\tilde{\omega}\tau. \tag{19}$$

Using complex representation $\psi = \mathrm{Re}[\psi_\omega\exp(-i\tilde{\omega}\tau)]$, we obtain a solution

$$\psi_\omega = \frac{ig_m}{\tilde{\omega}^2 - \tilde{\omega}_m^2 + i(\nu_c+\nu_r)\tilde{\omega}}, \tag{20}$$

where

$$\nu_r = \frac{4\beta_\omega}{L} = \frac{2L_z\omega}{\varepsilon_c L\omega_p} \tag{21}$$

is the parameter of the radiation damping (the last formula is written in real units). One can see that both the quasiparticle dissipation and radiation contribute to the resonance damping.[27] The cavity quality factor is given by $Q_c = \omega_m/(\nu_c+\nu_r)$. Optimal power conversion is achieved when the main contribution to damping comes from the radiation, $\nu_c \ll \nu_r$. Comparing the damping channels using Eq. (7), we obtain that this is achieved for a sufficiently large number of junctions in the stack

$$N > N_\sigma = \frac{\varepsilon_c\nu_c L}{2s\tilde{\omega}} = \frac{2\pi\sigma_c L}{\omega s}. \tag{22}$$

Taking $s = 1.56$ nm, we also rewrite this formula in the practically convenient form as

$$N_\sigma \approx 576\sigma_c[1/(\Omega\ \mathrm{cm})]L[\mu\mathrm{m}]/f[\mathrm{THz}].$$

For typical values $\sigma_c = 0.003-0.01\ (\Omega\ \mathrm{cm})^{-1}$, $L \sim 40\ \mu$m, and $f = \omega/2\pi = 1$ THz, we estimate $N_\sigma = 70-250$. In the regime of dominating radiation losses, the cavity quality factor is simply given by $Q_c = \varepsilon_c L/2L_z$.

The solution (20) allows us to obtain the average JCC

$$i_J = \langle g(x)\sin\{\tilde{\omega}\tau + \mathrm{Re}[\psi_\omega \exp(-i\tilde{\omega}\tau)]\cos(m\pi x/L)\}\rangle = \frac{1}{4}\frac{g_m^2(\nu_c+\nu_r)\tilde{\omega}}{[\tilde{\omega}^2-\tilde{\omega}_m^2]^2+(\nu_c+\nu_r)^2\tilde{\omega}^2}. \quad (23)$$

This gives the maximum current enhancement in the resonance

$$i_{J,\max} = \frac{g_m^2/4}{(\nu_c+\nu_r)\tilde{\omega}_m}. \quad (24)$$

A similar result has been derived in Ref. 24 for the case of a single junction without radiation losses. Comparing this result with the reduced quasiparticle current, $\nu_c\tilde{\omega}$, we see that the resonance feature in $I$-$V$ characteristic is pronounced if $g_m > 2\sqrt{(\nu_c+\nu_r)\nu_c\tilde{\omega}}$. In the case of dominating radiation losses, we can rewrite this condition in a more transparent form, $g_m > 2\sqrt{2L_z\nu_c/\varepsilon_c L}\tilde{\omega}^{3/2}$. For $\nu_c=0.01$, $\tilde{\omega}=10$, $L_z=1.5$ $\mu$m, and $L=40$ $\mu$m corresponding to $m=1$, we obtain that the resonance feature in the $I$-$V$ dependence becomes strong when the coupling parameter exceeds 0.5. In the case of strong resonance, the total current $i(\tilde{\omega})=\nu_c\tilde{\omega}+i_J$ nonmonotonically depends on the Josephson frequency $\tilde{\omega}$ (voltage). In this case, only the increasing part $di/d\tilde{\omega}>0$ is stable.

The total radiated power from both sides is given by

$$P_{\mathrm{tot}}(\omega) = 2P_{\mathrm{sc}}\frac{\partial\psi}{\partial\tau}\hat{\beta}\frac{\partial\psi}{\partial\tau} = 2P_{\mathrm{sc}}\,\mathrm{Re}[\beta_\omega]\tilde{\omega}^2|\psi_\omega|^2 = \frac{2P_{\mathrm{sc}}\beta_\omega\tilde{\omega}^2 g_m^2}{[\tilde{\omega}^2-\tilde{\omega}_m^2]^2+(\nu_c+\nu_r)^2\tilde{\omega}^2}. \quad (25)$$

Here, the scale of $P_{\mathrm{tot}}$ is given by $P_{\mathrm{sc}}=L_yL_z\lambda_c E_p j_J/2$, where $E_p=\Phi_0\omega_p/2\pi cs$ is the electric field corresponding to the plasma frequency. For the maximum radiated power in the resonance, we obtain $P_{\mathrm{tot}}(\omega_m)=2P_{\mathrm{sc}}\beta_\omega g_m^2/(\nu_c+\nu_r)^2$. In the regime of dominating radiation losses, $\nu_c \ll \nu_r$, using Eq. (7) and $j_J=c\Phi_0/8\pi^2 s\lambda_c^2$, we obtain a very simple and universal estimate for maximum total radiated power (in real units)

$$P_{\mathrm{tot}}(\omega_m) \approx \frac{\pi L_y L^2 g_m^2 j_J^2}{2\omega}. \quad (26)$$

An important observation is that *for a tall stack in resonance, the radiated power does not depend on N* due to compensation between the factor $N^2$ in front of the radiated power (8) and the amplitude of phase oscillations in the resonance, which, due to the increasing radiation losses, drops as $\zeta^{-2} \propto N^{-2}$ (see also Ref. 19). This compensation only exists in the regime when the damping of the resonance is caused by the radiation which is realized under the condition (22).

The power conversion efficiency is given by

$$Q = \frac{P_{\mathrm{tot}}}{L(i_J+\nu_c\tilde{\omega})\tilde{\omega}}. \quad (27)$$

In resonance, it can be represented in a quite transparent form as a product of two factors

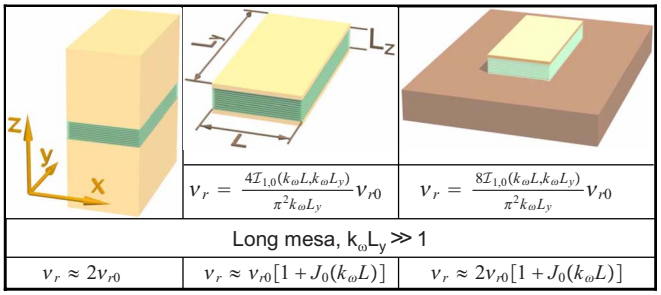


FIG. 2. (Color online) The parameter of radiation damping for the fundamental mode for different mesa designs in the case $k_\omega L_z \ll 1$: long mesa with screens mostly considered in the paper (left), rectangular capacitor (middle), and mesa with ground plate (e.g., mesa fabricated on the top of bulk crystal) (right). Here, $\nu_{r0}=\omega L_z/\varepsilon_c\omega_p L$ and the function $\mathcal{I}_{1,0}(a_x,a_y)$ is defined in Appendix B [Eq. (B8)]. In the regime of dominating radiation losses, the cavity quality factor $Q_c$ is directly determined by $\nu_r$ as $Q_c=\omega/\nu_r\omega_p$.

$$Q_r = \frac{g_m^2}{g_m^2+4(\nu_c+\nu_r)\nu_c\tilde{\omega}^2}\frac{\nu_r}{\nu_c+\nu_r}, \quad (28)$$

where the first factor represents the relative current increase in the resonance, $i_{J,\max}/(\nu_c\tilde{\omega}+i_{J,\max})$, and the second factor is the relative contribution of the radiation to the resonance damping. We can see that, remarkably, in resonance the conversion efficiency can approach 100% provided (i) the resonance feature is pronounced in $I$-$V$ dependence, $g_m > 2\sqrt{(\nu_c+\nu_r)\nu_c\tilde{\omega}}$, and (ii) the losses are dominated by the radiation, $\nu_c < \nu_r$. Both conditions are quite realistic.

Remember that simple and transparent results for the typical number of junctions [Eq. (22)], current [Eq. (24)], radiation power [Eq. (26)], and conversion efficiency [Eq. (28)] are valid only in the case $\omega L_y/c > 1$ and without mixing of radiation coming from the opposite sides. These results can be generalized for other cases. Radiation losses of the resonance mode in the short rectangular mesa can be approximately calculated similar to radiation out of a rectangular capacitor.[28] These calculations are summarized in Appendix B, and the results for the radiation damping parameter for different cases are presented in Fig. 2. In the case of long mesas, $k_\omega L_y \gg 1$, the radiation damping parameters for different geometries differ only by numerical factors of order unity. In the opposite limit, $k_\omega L_y \ll 1$, $\nu_r$ acquires an additional small factor $\sim k_\omega L_y$.

## V. SPECIAL CASES OF MODULATION

In this section, we consider several special cases of modulation for which the problem allows for exact analytical solution and full analysis of transport and radiation properties. We will consider three cases: linear modulation, parabolic modulations, and steplike suppression of the critical current. Practical ways to prepare such modulations are suggested Sec. VI.

### A. Linear modulation

In this section, we consider a mesa with linearly modulated JCC, $g(x)=1-2r\bar{x}/L$ [see Fig. 1(a)]. Here, we intro-

duce the new coordinate $\bar{x}=x-L/2$, which is symmetrical with respect to the mesa, $-L/2<\bar{x}<L/2$. This means that the JCC at the left side is larger by a factor $(1+r)/(1-r)$ than the JCC at the right side. Such a modulation couples homogeneous Josephson oscillations with the odd Fiske modes (1), $m=2l+1$, including the fundamental mode, $m=1$, and the coupling parameter (18) to this mode is connected with the modulation parameter as

$$g_1 = 8r/\pi^2. \tag{29}$$

Solution of Eq. (4) with the boundary conditions (6) in the case of linear modulation can be found exactly. Splitting the solution into the symmetric and antisymmetric parts, $\theta_\omega(\bar{x}) = \theta_\omega^{(a)}(\bar{x}) + \theta_\omega^{(s)}(\bar{x})$, we derive

$$\theta_\omega^{(a)}(\bar{x}) = -\frac{2ir\bar{x}/L}{\tilde{\omega}^2 + i\nu_c\tilde{\omega}} + \frac{(2i/L+\zeta)r\sin(p_\omega\bar{x})}{(\tilde{\omega}^2 + i\nu_c\tilde{\omega})[p_\omega\cos(\chi) - i\zeta\sin(\chi)]}, \tag{30}$$

$$\theta_\omega^{(s)}(\bar{x}) = \frac{i}{\tilde{\omega}^2 + i\nu_c\tilde{\omega}} + \frac{\zeta\cos(p_\omega\bar{x})}{(\tilde{\omega}^2 + i\nu_c\tilde{\omega})[p_\omega\sin(\chi) + i\zeta\cos(\chi)]}, \tag{31}$$

with

$$p_\omega^2 \equiv \tilde{\omega}^2 + i\nu_c\tilde{\omega} \quad \text{and} \quad \chi \equiv p_\omega L/2.$$

Only the antisymmetric phase is coupled to the resonance mode. In particular, for the boundary phases, we have

$$\theta_\omega^{(a)}\left(\pm\frac{L}{2}\right) = \pm\frac{ir[-\cos(\chi)+\sin(\chi)/\chi]}{p_\omega[p_\omega\cos(\chi) - i\zeta\sin(\chi)]}, \tag{32}$$

$$\theta_\omega^{(s)}\left(\pm\frac{L}{2}\right) = \frac{i\sin(\chi)}{p_\omega[p_\omega\sin(\chi) + i\zeta\cos(\chi)]}. \tag{33}$$

The radiated power is determined by the boundary phases using Eq. (8), where we have to replace $\theta_\omega(0)$ with $\theta_\omega^{(a)}(\pm L/2) + \theta_\omega^{(s)}(\pm L/2)$.

Near the resonance $\tilde{\omega}L=\pi$, using $p_\omega \approx \tilde{\omega} + i\nu_c/2$ and $\cos(\chi) \approx (\pi/2 - \tilde{\omega}L/2) - i\nu_c L/4$, we obtain

$$\theta_\omega^{(a)}\left(\frac{L}{2}\right) \approx -\frac{8ir/\pi^2}{(\tilde{\omega}+i\nu_c)[2(\tilde{\omega}-\pi/L) + i(\nu_c+\nu_r)]},$$

where $\nu_r$ is defined in Eq. (21). Using the coupling parameter (29), we can see that this result is consistent with the general formula (20) near the resonance. The maximum antisymmetric phase in the resonance can be estimated as $\theta_\omega^{(a)}(L/2) \approx -2r/\pi\beta_\omega\tilde{\omega}^2$. It exceeds the nonresonant symmetric part approximately by a factor $r/\beta_\omega \approx r\varepsilon_c L/L_z$. In resonance, using Eqs. (26) and (29), we obtain for the radiation power from one side in real units

$$P_r \approx L_y \frac{16r^2L^2j_J^2}{\pi^3\omega}.$$

It exceeds nonresonant emission by a factor $(r\varepsilon_c L/L_z)^2$. In particular, for $\omega/2\pi=1$ THz, $j_J=500$ A/cm$^2$, and $r=0.4$, we estimate $P_r/L_y \approx 0.05$ W/cm.

In the average JCC (10), the contributions from symmetric and antisymmetric parts split, $i_J = i_{J,a} + i_{J,s}$. Direct calculation gives

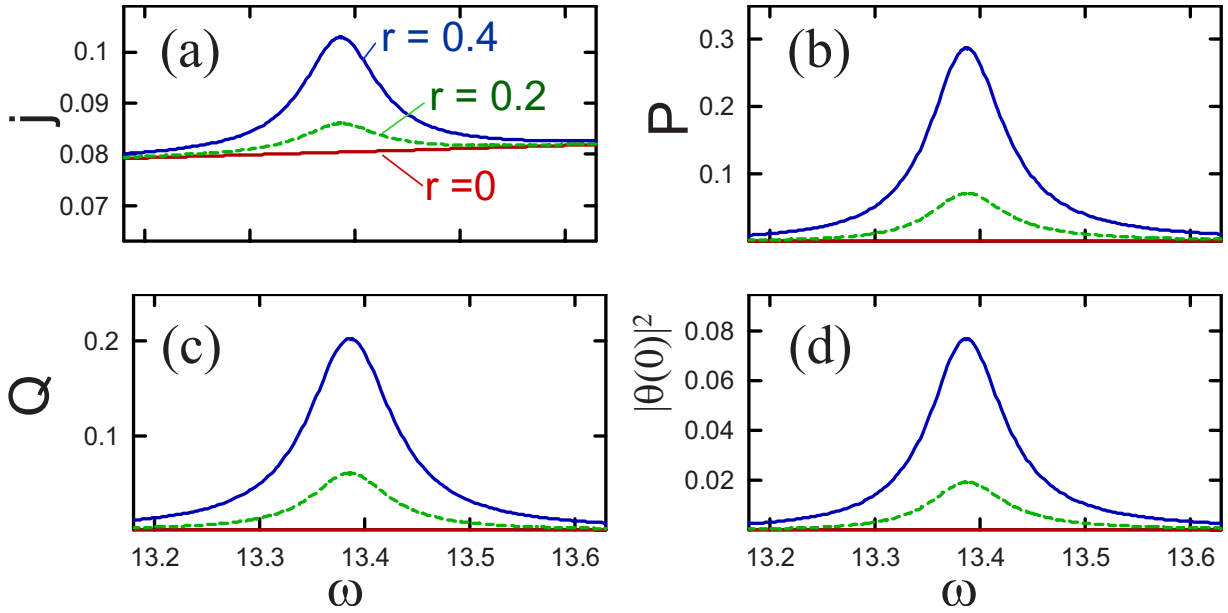


FIG. 3. (Color online) Representative plots of the Josephson-frequency (or voltage) dependences of (a) the current density $j$, (b) radiated power from the left side, $P$, (c) power conversion efficiency $Q$, and (d) amplitude of oscillating phase at the boundary for stacks with linearly modulated JCC with parameters $r=0.2$ and $r=0.4$. The unit of current density is the JCC density, $j_J$, the frequency unit is the plasma frequency $\omega_p$, and the unit of radiated power is $10^{-3}P_J$ [see Eq. (36)], corresponding to $P/L_y \sim 0.16$ W/cm. The following parameters have been used: $L=0.23$, $\nu_c=0.006$, and $\mathrm{Re}[\zeta]=0.00035\tilde{\omega}^2$. For comparison, the case of homogeneous JCC ($r=0$) is also shown, but $P$, $Q$, and $|\theta|^2$ are indistinguishable from zero at the scales of the plots. In this case, $P \approx 1.1\times10^{-4}$ and $Q \approx 10^{-4}$ at $\omega=13.4$.

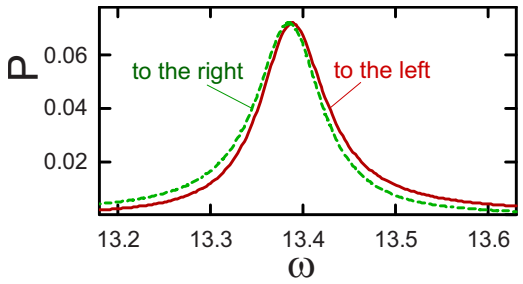


FIG. 4. (Color online) Comparison between the powers radiated to the two opposite sides of the mesa for $r=0.2$ and the same parameters as in the previous figure. One can see that the difference is rather small and amounts to a slightly different asymmetry of the peaks.

$$i_{J,a} = \frac{r^2}{2}\left\{ \frac{\nu_c/3}{(\tilde{\omega}^2+\nu_c^2)\tilde{\omega}} + \mathrm{Re}\left[ \frac{[\cos(\chi)-\sin(\chi)/\chi](2i/L+\zeta)/\chi}{(\tilde{\omega}^2+i\nu_c\tilde{\omega})[p_\omega\cos(\chi)-i\zeta\sin(\chi)]} \right] \right\}, \quad (34)$$

$$i_{J,s} = \frac{1}{2}\mathrm{Re}\left[ \frac{i}{\tilde{\omega}^2+i\nu_c\tilde{\omega}} \left( 1 - \frac{2i\zeta\sin(\chi)/L}{p_\omega\sin(\chi)+i\zeta\cos(\chi)} \right) \right]. \quad (35)$$

From the general formula for $i_{J,a}$ near the resonance, we obtain a much simpler result

$$i_{J,a} \approx \frac{16r^2}{\pi^4} \frac{(\nu_c+\nu_r)/\tilde{\omega}}{4(\tilde{\omega}-\pi/L)^2+(\nu_c+\nu_r)^2},$$

and the maximum current enhancement in the resonance is given by

$$i_{J,a} \approx \frac{16r^2/\pi^4}{\tilde{\omega}(\nu_c+\nu_r)}.$$

These results are also consistent with the corresponding general formulas (23) and (24) if we use the coupling parameter (29). For comparison, the symmetric part of the JCC at the resonance frequency can be estimated as

$$i_{J,s} \approx \frac{\nu_c}{2\tilde{\omega}^3} + \frac{\beta_\omega}{\pi\tilde{\omega}^2}.$$

As expected, the resonant enhancement of the current exceeds the nonresonant radiation correction by the same factor $(r/\beta_\omega)^2=(r\varepsilon_c L/L_z)^2$ as for the radiation power.

For illustration, we present the behavior near the resonance for mesas with two modulation parameters, $r=0.2$ and $r=0.4$. As a unit of the radiation power, we selected the quantity

$$P_J = L_y\lambda_c^2 j_J^2/\omega_p, \quad (36)$$

which is independent of the sizes $L$ and $L_z$. This choice of unit is suggested by the result (26). For $\lambda_c=185$ $\mu$m, $P_J/L_y \approx 163$ W/cm. Figure 3 shows the Josephson-frequency dependences of (i) the current density $j$ (in units of the JCC density in the center), (ii) radiated power $P$ (in units of $10^{-3}P_J$), (iii) the power conversion efficiency $Q$, and (iv) the amplitude of oscillating phase at the boundary. For comparison, the case of homogeneous mesa ($r=0$) is also shown. In calculation, we used the following parameters: $L=0.23$, $\nu_c=0.006$, and $\mathrm{Re}[\zeta]=0.00035\tilde{\omega}^2$ (corresponding to $N\approx 1000$, $\lambda_c\approx 185$ $\mu$m, and $\sigma_c\approx 0.003$ $[\Omega\,\mathrm{cm}]^{-1}$). We can see that the modulation leads to the appearance of a strong resonance feature in the $I$-$V$ dependence. Note that only $I$-$V$ regions with positive differential resistivity are stable. Current enhancement in the resonance is mainly caused by the generation of the powerful electromagnetic wave, and it is accompanied by a huge enhancement of outside radiation. The maximum radiation power for used parameters for the case $r=0.4$ corresponds to $\sim 0.05$ W/cm, and it exceeds the nonresonant radiation from the homogeneous mesa by more than 3 orders of magnitude. It is important to note that the power conversion efficiency is also strongly enhanced in the resonance, reaching 20% for $r=0.4$. The plot of $|\theta|^2$ shows that for selected parameters, it remains smaller than 1 in the resonance and, therefore, the linear approximation used in calculations is not violated.

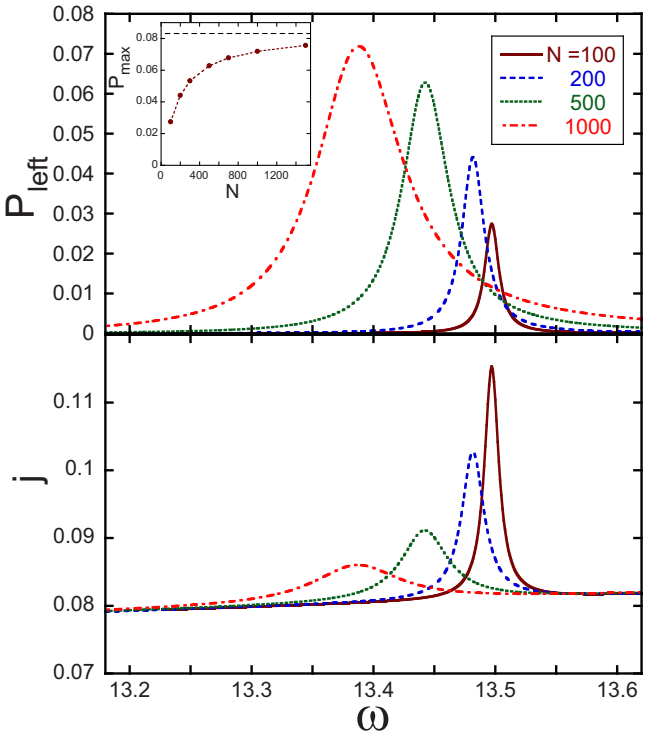


FIG. 5. (Color online) Evolution of the radiation power and resonance feature in the $I$-$V$ dependence with increasing number of junctions in the stack, $N$, for $r=0.2$ and the same parameters as in Fig. 3. Note that while the radiation power increases with $N$, the resonant feature in current becomes less pronounced due to the increasing radiation damping $\propto N^2$. The inset in the upper plot shows the $N$ dependence of the maximum radiation power, and the dashed line in this plot indicates the large-$N$ limit obtained from Eq. (26).

In spite of the asymmetry of the JCC, the powers radiated to the opposite sides of the mesa in resonance are approximately the same, because the radiation is mostly promoted by the resonance mode which has identical amplitudes of the

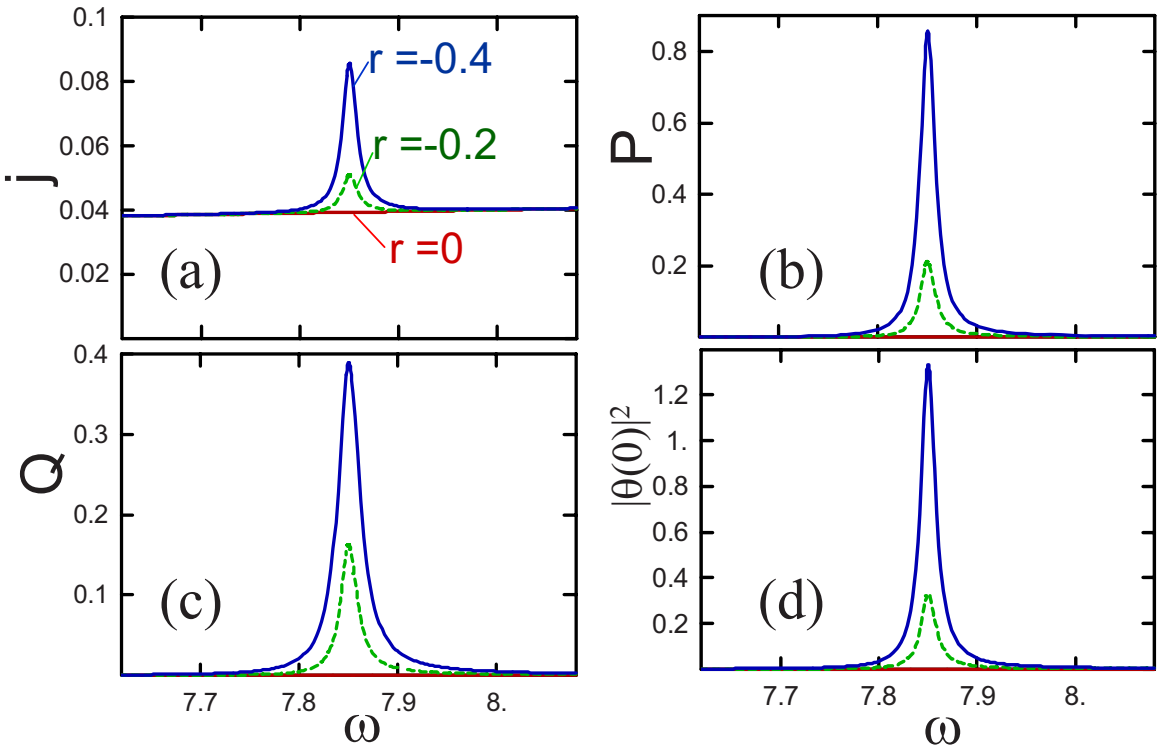


FIG. 6. (Color online) The Josephson-frequency (or voltage) dependences of (a) the current density $j$, (b) radiated power to one side $P$, (c) power conversion efficiency $Q$, and (d) amplitude of the oscillating phase at the boundary for stacks with parabolic profiles of the JCC and negative modulation parameters, $r=-0.2$ and $r=-0.4$, corresponding to the case of current enhancement at the edges. All units are the same as in Fig. 3. The following parameters have been used: $L=0.8$, $\nu_c=0.005$, and $\mathrm{Re}[\tilde{\zeta}]=0.003\tilde{\omega}^2$, corresponding to $N\approx 1000$ and $\lambda_c \approx 200$ $\mu$m in the middle. For comparison, the case of a homogeneous mesa ($r=0$) is also shown. In this case, $P\approx 5\times 10^{-5}$ and $Q\approx 5\times 10^{-5}$ at $\omega=7.85$.

oscillating electric field at the opposite sides. This is illustrated in Fig. 4, where these powers are plotted for $r=0.2$. One can see that the peaks have slightly different asymmetries originating from the symmetric phase.

Figure 5 illustrates the evolution of the radiation power and resonance feature in the $I$-$V$ dependence with increasing number of junctions in the stack, $N$, for $r=0.2$ and the same parameters as in Fig. 3. The number of junctions above which the radiation losses dominate [Eq. (22)] can be estimated for used parameters as $N_\sigma \approx 75$. We can see that the current and radiation have opposite tendencies: while the radiation power increases with $N$, the resonant feature in current becomes less pronounced due to the increasing radiation damping.

### B. Symmetric parabolic modulation

In this section, we consider a symmetric modulation. For simplicity, we assume a simple parabolic profile of the JCC density, $g(\bar{x})=1-r(2\bar{x}/L)^2$ [see Fig. 1(b)] where, again, $\bar{x}=x-L/2$ and $1-r$ is the ratio of JCCs at the edge and in the center. The cases $r>0$ and $r<0$ correspond to current suppression and enhancement at the edges, respectively. Such a modulation will lead to excitation of only even frequency modes (1), $m=2l$. In the following, we will focus on the lowest even mode with $m=2$. To have this resonance at $\omega_2/2\pi=1$ THz assuming $\varepsilon_c \approx 12$, the mesa size has to be rather large, $L=86.5$ $\mu$m. The coupling parameter (18) to this mode in our case is given by

$$g_2 = -4r/\pi^2. \tag{37}$$

The oscillating phase in the case of parabolic modulation also can be found exactly. From symmetry, the solution of Eq. (4) with boundary conditions (6) must be an even function of $\bar{x}$, and it has the following form:

$$\theta_\omega = \frac{2ir(2/L)^2}{(\tilde{\omega}^2+i\nu_c\tilde{\omega})^2} + \frac{i[1-r(2\bar{x}/L)^2]}{\tilde{\omega}^2+i\nu_c\tilde{\omega}} + C\cos(p_\omega \bar{x}), \tag{38}$$

where the first two terms give a particular solution of the inhomogeneous equation and the last term is the solution of the homogeneous equations. From the boundary conditions (6), we obtain

$$C = \frac{-4ir/L + \zeta(2r/\chi^2+1-r)}{[p_\omega \sin(\chi)+i\zeta\cos(\chi)](\tilde{\omega}^2+i\nu_c\tilde{\omega})}, \tag{39}$$

where $p_\omega$ and $\chi$ are defined after Eq. (31). The oscillating phase given by Eqs. (38) and (39) determines all other observable properties.

The powers radiated from both sides [Eq. (8)] are determined by the boundary phase $\theta_{\omega,0}=\theta_\omega(\bar{x}=\pm L/2)$, which we obtain from Eqs. (38) and (39),

$$\theta_{\omega,0} = \frac{2ir(2/L)^2}{(\tilde{\omega}^2 + i\nu_c\tilde{\omega})^2} + \frac{i(1-r)}{\tilde{\omega}^2 + i\nu_c\tilde{\omega}} + \frac{[-4ir/L + \zeta(2r/\chi^2 + 1 - r)]\cos(\chi)}{[p_\omega \sin(\chi) + i\zeta\cos(\chi)](\tilde{\omega}^2 + i\nu_c\tilde{\omega})}.$$

In the resonance, $\tilde{\omega}L = 2\pi$, using $\theta_\omega(L/2) \approx -2r/(\pi\zeta\tilde{\omega})$, we obtain for the power radiated from one side in real units

$$P(\omega_2) \approx \frac{4L_y L^2 r^2 j_J^2}{\pi^3 \omega}. \tag{40}$$

This result is consistent with the general formula (26), with the coupling parameter (37). For $\omega/2\pi = 1$ THz, $j_c = 500$ A/cm$^2$, and $r = \pm 0.5$, we obtain an estimate for the radiated power in the resonance, $P/L_y \approx 0.085$ W/cm. Note that $j_J$ in Eq. (40) is the JCC density in the center, while the the JCC density at the edge, $j_{J,e}$, is given by $j_{J,e} = (1-r)j_J$. In the case of $r < 0$, vanishing of superconductivity in the middle, which corresponds to the limits $j_J \to 0$ and $r \to -\infty$, does not lead to vanishing of radiation power because $r^2 j_J^2 \to j_{J,e}^2$ and the radiation is determined by the JCC density at the edge.

To find the voltage-current characteristic, we calculate the average reduced JCC (10). Using oscillating phase (38), we obtain

$$i_J = \frac{\nu_c}{2\tilde{\omega}(\tilde{\omega}^2 + \nu_c^2)}\left[1 - \frac{2r}{3} + \frac{r^2}{5} + \frac{16r/L^2}{\tilde{\omega}^2 + \nu_c^2}\left(1 - \frac{r}{3}\right)\right] + \mathrm{Re}\left\{\frac{C}{2}\left(\frac{\sin\chi}{\chi} - 2r\left[\left(1 - \frac{2}{\chi^2}\right)\frac{\sin\chi}{2\chi} + \frac{\cos\chi}{\chi^2}\right]\right)\right\}. \tag{41}$$

At the resonance frequency, $\tilde{\omega}L = 2\pi$, we estimate $i_J \approx \varepsilon_c r^2 L^3/2\pi^6 L_z$.

Figure 6 shows the representative Josephson-frequency dependences of the current density $j$, radiated power $P$ to one side, the power conversion efficiency $Q$, and the amplitude of oscillating phase at the boundary for negative modulation parameters, $r = -0.2$ and $r = -0.4$, corresponding to the case of stronger superconductivity at the edges. In calculation, we used the following parameters: $L = 0.8$, $\nu_c = 0.005$, and $\mathrm{Re}[\zeta] = 0.003\tilde{\omega}^2$ (corresponding to $N \approx 1000$ and $\lambda_c \approx 200$ $\mu$m in the center). Overall, the behavior is very similar to the case of linear modulation shown in Fig. 3 with minor quantitative differences. We also see that the modulation leads to the appearance of a strong resonance feature in the $I$-$V$ dependence accompanied by a huge enhancement of the outside radiation and power conversion efficiency.

### C. Steplike suppression of critical current near the edge

In this section, we consider the case when there is a region with suppressed JCC on one side [see Fig. 1(c)]

$$g(x) = \begin{cases} 1 & \text{for } 0 < x < L - W \\ 1 - r & \text{for } L - W < x < L. \end{cases} \tag{42}$$

The coupling parameter (18) to the fundamental mode in this case is given by

$$g_1 = \frac{2r}{\pi}\sin\left(\frac{\pi W}{L}\right). \tag{43}$$

The solution of equation for the oscillating phase (4) can be built in the piecewise form

$$\theta_\omega = \begin{cases} i/(\tilde{\omega}^2 + i\nu_c\tilde{\omega}) + A_+ \exp(ip_\omega x) + A_- \exp(-ip_\omega x) \\ \text{for } 0 < x < L - W \\ i(1-r)/(\tilde{\omega}^2 + i\nu_c\tilde{\omega}) + (A_+ - C_+)\exp(ip_\omega x) + (A_- - C_-)\exp(-ip_\omega x) \\ \text{for } L - W < x < L, \end{cases} \tag{44}$$

with $p_\omega^2 \equiv \tilde{\omega}^2 + i\nu_c\tilde{\omega}$. Matching $\theta_\omega$ and $d\theta_\omega/dx$ at $x = L - W$, we obtain

$$C_\pm = \frac{-ir/2}{\tilde{\omega}^2 + i\nu_c\tilde{\omega}} \exp[\mp ip_\omega(L - W)]. \tag{45}$$

Using this result, from the boundary conditions (6) we find the coefficients $A_\pm$,

$$A_\pm = \frac{\zeta\{(p_\omega \pm \zeta)\exp(\mp i\bar{\chi}) + (p_\omega \mp \zeta)[1 - r(1 - \cos\eta)]\} - irp_\omega(p_\omega \mp \zeta)\sin\eta}{2(\tilde{\omega}^2 + i\nu_c\tilde{\omega})\{[p_\omega^2 + \zeta^2]\sin\bar{\chi} + 2ip_\omega\zeta\cos\bar{\chi}\}}, \tag{46}$$

where $\bar{\chi} \equiv p_\omega L$ and $\eta \equiv p_\omega W$. This gives, for the boundary phases which determine the outside radiation,

$$\theta_\omega(0) = \frac{i}{\tilde{\omega}^2 + i\nu_c\tilde{\omega}} + \frac{\zeta\{p_\omega[1 + \cos\bar{\chi}] - i\zeta\sin\bar{\chi}\} - rp_\omega\{\zeta(1 - \cos\eta) + ip_\omega\sin\eta\}}{(\tilde{\omega}^2 + i\nu_c\tilde{\omega})[(p_\omega^2 + \zeta^2)\sin\bar{\chi} + 2ip_\omega\zeta\cos\bar{\chi}]}, \tag{47}$$

$$\theta_\omega(L)=\frac{i\{1-r(1-\cos\ \eta)\}}{\tilde{\omega}^2+i\nu_c\tilde{\omega}}+\frac{\zeta[p_\omega(1+\cos\ \bar{\chi})-i\zeta\sin\ \bar{\chi}]-r[\zeta(1-\cos\ \eta)+ip_\omega\sin(\eta)][p_\omega\cos\ \bar{\chi}-i\zeta\sin\ \bar{\chi}]}{(\tilde{\omega}^2+i\nu_c\tilde{\omega})\{[p_\omega^2+\zeta^2]\sin\ \bar{\chi}+2ip_\omega\zeta\cos\ \bar{\chi}\}}. \quad (48)$$

Near the resonance, $\tilde{\omega}L=\pi$, the coefficients $A_+$ and $A_-$ can be strongly simplified

$$A_+\approx A_-\approx\frac{-ir\sin[\tilde{\omega}W]/2\omega^2}{2(\tilde{\omega}-\pi/L)-i(\nu_c+\nu_r)}.$$

In the resonance, $A_+\approx A_-\approx r\sin[\tilde{\omega}W]/4\tilde{\omega}^2\beta_\omega$, giving

$$\theta_\omega(0)\approx\frac{i}{\tilde{\omega}^2+i\nu_c\tilde{\omega}}+\frac{r\sin[\tilde{\omega}W]}{2\tilde{\omega}\beta_\omega}.$$

At $W\ll L$, the resonance is strong, $\theta_\omega(0)>1$, if $rW\gg 2\tilde{\omega}\beta_\omega$ or, in real units,

$$rW\gg\frac{\pi^2\lambda_c^2L_z}{\varepsilon_cL^2}.$$

The total radiated power in resonance can be estimated as

$$P_{\rm tot}(\omega_1)\approx\frac{2L_yL^2j_J^2r^2\sin^2(\pi W/L)}{\pi\omega}, \quad (49)$$

which is consistent with the general formula (26).

The reduced JCC flowing through the stack (10) can be computed as

$$i_J=\frac{[L-r(2-r)W]\nu_c}{2L(\tilde{\omega}^2+\nu_c^2)\tilde{\omega}}-\frac{(1-r)r}{2L}\,{\rm Im}\left[\frac{\sin\ \eta}{p_\omega^3}\right]+{\rm Re}\left[\frac{\mathcal{N}/\bar{\chi}}{(\tilde{\omega}^2+i\nu_c\tilde{\omega})\{[p_\omega^2+\zeta^2]\sin\ \bar{\chi}+2ip_\omega\zeta\cos\ \bar{\chi}\}}\right], \quad (50)$$

with

$$\mathcal{N}=\left(p_\omega\cos\frac{\bar{\chi}}{2}-i\zeta\sin\frac{\bar{\chi}}{2}\right)\left\{\zeta\sin\frac{\bar{\chi}}{2}-r\sin\frac{\eta}{2}\left[\zeta\cos\frac{\eta}{2}+i\left(p_\omega\cos\frac{\eta}{2}-i\zeta\sin\frac{\eta}{2}\right)\sin\frac{\bar{\chi}}{2}\right]\right\}+ir^2\sin^2\frac{\eta}{2}\left(p_\omega\cos\frac{\eta}{2}-i\zeta\sin\frac{\eta}{2}\right)\left(p_\omega\cos\left[\bar{\chi}-\frac{\eta}{2}\right]+i\zeta\sin\left[\bar{\chi}-\frac{\eta}{2}\right]\right).$$

Near the resonance, we estimate $\mathcal{N}\approx -ip_\omega^2r^2\sin^2(\tilde{\omega}W)/2$, which gives

$$i_J\approx\frac{r^2\sin^2(\tilde{\omega}W)\{\nu_cL/2+2\beta_\omega\}/2\pi}{\omega^2\{\sin^2(\tilde{\omega}L)+(\nu_cL/2+2\beta_\omega)^2\}}. \quad (51)$$

The maximum current enhancement in the resonance is given by

$$i_{J,\max}\approx\frac{r^2\sin^2(\pi W/L)}{\pi^2\tilde{\omega}(\nu_c+4\beta_\omega/L)}$$

in agreement with Eqs. (24) and (43).

General cumbersome formulas (47), (48), and (50) can be significantly simplified if we assume the conditions $\nu_c$, $|\zeta|\ll\omega$ and $W\ll L$ valid in most practical situations. In this case, these equations can be represented in approximate, simpler form,

$$\theta_\omega(0)\approx\frac{i}{\tilde{\omega}^2+i\nu_c\tilde{\omega}}-\frac{irW/\tilde{\omega}}{\sin\ \bar{\chi}-i(\nu_cL/2+2\beta_\omega)\cos\ \bar{\chi}}, \quad (52)$$

$$\theta_\omega(L)\approx\frac{i}{\tilde{\omega}^2+i\nu_c\tilde{\omega}}-\frac{irW\cos\ \bar{\chi}/\tilde{\omega}}{\sin\ \bar{\chi}-i(\nu_cL/2+2\beta_\omega)\cos\ \bar{\chi}}, \quad (53)$$

and

$$i_J\approx\nu_c\tilde{\omega}+\frac{\nu_c}{2\tilde{\omega}^3}-\frac{\nu_crW}{2L\tilde{\omega}^3}+{\rm Re}\left\{\frac{2\beta_\omega\sin\ \bar{\chi}-i\tilde{\omega}{\rm rW}\left[\sin\ \bar{\chi}-2i\beta_\omega\left[\cos\left(\bar{\chi}-\frac{\eta}{2}\right)+\cos\left(\frac{\eta}{2}\right)\right]-2\tilde{\omega}rW\cos\left(\bar{\chi}-\frac{\eta}{2}\right)\right]}{2L\tilde{\omega}^3[\sin\ \bar{\chi}-i(\nu_cL/2+2\beta_\omega)\cos\ \bar{\chi}]}\right\}$$

with $\bar{\chi}\approx\tilde{\omega}L$ and $\eta\approx\tilde{\omega}W$.

Figure 7 illustrates the evolution of the radiated power and resonance feature in the $I$-$V$ dependence with increasing width of the suppressed region. The JCC density in the suppressed region is assumed to be half of its value in the rest part, $r=0.5$. For used parameters, the maximum radiation power in this plot is around $P_{\max}/L_y\sim 0.05$ W/cm.

## VI. DISCUSSION AND SUMMARY

Let us discuss now practical ways to prepare mesas with lateral modulation of the critical current density. Mesas with linear JCC modulation can be fabricated in a crystal with inhomogeneous doping. One possible way to prepare such inhomogeneity is to utilize the sensitivity of doping in BSCCO to the oxygen concentration. Due to strong tempera-

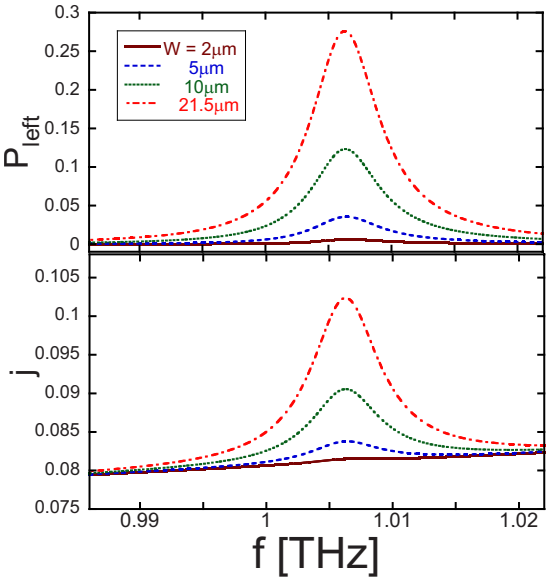


FIG. 7. (Color online) The radiated power and *I-V* dependence near the resonance for different widths of the suppressed region near the right side of the mesa. The JCC density in the suppressed region is assumed to be half of its value in the rest part, $r=0.5$. All units and parameters are the same as in Fig. 3.

ture dependence of the oxygen diffusivity,[29] in principle, the oxygen concentration profile in the crystal can be prepared by short-time annealing by carefully selecting the annealing temperature and time. In a similar way, mesas with paraboliclike profiles can be prepared by short-time annealing of mesas themselves already after fabrication. Another way to prepare modulation in a controlled way is to use radiation with high-energy electrons, protons, or heavy ions. If part of the mesa is protected by a mask, this radiation will produce a mesa with steplike suppression of the critical current.

The major technical challenge is to prepare a mesa with significant modulation of the Josephson coupling *identical in all junctions*. Variation of parameters in different junctions, which may be caused by composition variations, inhomogeneous heating, and different junction areas, would strongly reduce the optimal performance. The quantitative analysis of the radiation properties of mesas with such parameter variations in different layers will be done elsewhere.

As the optimal mesa size is rather large, another major technical problem is sample heating due to quasiparticle damping. The self-heating in the BSCCO mesas has been investigated by many experimental groups.[30] The major focus of these studies was the influence of heating on the gap feature in *I-V* characteristics, which is located at voltages of 30–60 mV/junction. Even though our voltage range is significantly lower, ~2 mV/junction, the heating is still expected to be significant due to the required large lateral size of the mesa. For example, for $\sigma_c=0.003\ 1/\Omega$ cm, $N=1000$, and $L_y=300\ \mu$m, 10 mW of power will be dissipated inside the mesa. This heat has to be removed from the mesa faces. Therefore, efficient heat removal is crucial for operation of the device. Recent experimental observations of the resonant emission using underdoped BSCCO (Ref. 25) demonstrate that the heating effects can be manageable even in large-size mesas with lateral sizes of several hundred micrometers in the voltage range corresponding to the Josephson frequencies around 1 THz.

The designs with improved thermal management may include, for example, fabrication of underdoped mesas on the top of overdoped crystal, using massive gold contacts on the top and bottom of the mesa, and placing an insulator with high thermal conductivity, such as sapphire, in good thermal contact at the side of the mesa. From these considerations, mesas with asymmetric modulation look more preferable than ones with symmetric modulation, because they need a smaller lateral size for the lowest resonance mode. In the case of symmetric modulation, the design with suppression of the JCC in the middle, $r<0$, looks more practical for better thermal management. In fact, the material in the middle can even be made insulating, because this part is needed only to form almost standing wave at the working frequency. To excite resonance mode, it is sufficient to have superconducting regions only at the edges.

In conclusion, we demonstrated that a stack of the intrinsic Josephson junctions with modulated Josephson coupling represents a very powerful and efficient source of electromagnetic radiation at the resonance frequency set by its lateral size. Selecting this size, the generation frequency can be tuned to the terahertz range. Power levels up to several milliwatts look plausible in such structures.

## ACKNOWLEDGMENTS

A.E.K. would like to acknowledge very useful discussions and joint work on practical implementation of the device discussed in this manuscript with U. Welp, K. Gray, L. Ozyuzer, and C. Kurter. In Argonne, this work was supported by the Department of Energy under Contract No. DE-AC02-06CH11357. In the Los Alamos National Laboratory, this work was carried out under the auspices of the National Nuclear Security Administration of the Department of Energy under Contract No. DE-AC-06NA25396.

## APPENDIX A: BOUNDARY CONDITIONS FOR THE HOMOGENEOUS OSCILLATING PHASE

In this appendix, we consider the boundary conditions for the oscillating phase at the edges and the radiation power for a stack of intrinsic Josephson junctions. We will limit ourselves to the case when the oscillating phase is identical in all junctions. A more general case will be considered elsewhere. The oscillating phase $\theta_\omega$ defined by Eq. (3) is connected to the electric and magnetic fields by the Josephson relations

$$E_z=-\frac{i\omega\Phi_0}{2\pi cs}\theta_\omega, \tag{A1}$$

$$B_y=\frac{\Phi_0}{2\pi s}\nabla_x\theta_\omega. \tag{A2}$$

Therefore, the boundary conditions for the oscillating phase at the edges are determined by the relation between the fields

$E_z$ and $B_y$ in the outside media, which we assume to be monochromatic with time dependences $\propto\exp(-i\omega t)$.

Outside dielectric media at $|x-L/2|>L/2$ is characterized by the dielectric constant $\varepsilon_d$, and we assume only outgoing wave in this space. The Fourier components of fields with $|k_z|<\sqrt{\varepsilon_d}k_\omega$ propagate in the media, while the field components with $|k_z|>\sqrt{\varepsilon_d}k_\omega$ decay. In particular, for $E_z(\omega,x,k_z)$ at $x>L$, we have

$$E_z(\omega,x,k_z)=E_z(\omega,L,k_z)\exp[ik_x(\omega,k_z)(x-L)], \quad \text{(A3)}$$

with

$$k_x(\omega,k_z)=\begin{cases}\sqrt{\varepsilon_d k_\omega^2-k_z^2}\ \mathrm{sign}(\omega) & \text{for } |k_z|<\sqrt{\varepsilon_d}|k_\omega| \\ i\sqrt{k_z^2-\varepsilon_d k_\omega^2} & \text{for } |k_z|>\sqrt{\varepsilon_d}|k_\omega|.\end{cases} \quad \text{(A4)}$$

Other field components, $E_x$ and $B_y$, are also expressed via $E_z(\omega,L,k_z)$. First, $E_x(\omega,x,k_z)$ is obtained from Eq. (A3) and the Maxwell equation $\nabla\cdot\mathbf{E}=0$, and then $B_y(\omega,x,k_z)$ is obtained using the Maxwell equation $(\nabla\times\mathbf{E})_y=ik_\omega B_y$, leading to the following result:

$$B_y(\omega,x,k_z)=-E_z(\omega,L,k_z)\frac{\varepsilon_d k_\omega}{k_x(\omega,k_z)}\exp[ik_x(\omega,k_z)(x-L)]. \quad \text{(A5)}$$

This gives the relation between the fields at the boundary $x=L$,

$$B_y(L,k_z)=-\zeta(\omega,k_z)E_z(L,k_z),$$

$$\zeta(\omega,k_z)=\begin{cases}|k_\omega|\varepsilon_d/\sqrt{\varepsilon_d k_\omega^2-k_z^2} & \text{for } |k_z|<\sqrt{\varepsilon_d}|k_\omega| \\ -ik_\omega\varepsilon_d/\sqrt{k_z^2-\varepsilon_d k_\omega^2} & \text{for } |k_z|>\sqrt{\varepsilon_d}|k_\omega|.\end{cases} \quad \text{(A6)}$$

The condition at $x=0$ has opposite sign, $B_y(0,k_z)=\zeta(\omega,k_z)E_z(0,k_z)$. Note again that the term $\zeta(\omega,k_z)$ for $|k_z|<\sqrt{\varepsilon_d}k_\omega$ originates from outgoing electromagnetic wave (radiation), while the term $\zeta(\omega,k_z)$ for $|k_z|>\sqrt{\varepsilon_d}k_\omega$ is due to the wave decaying at distance $\sim(k_z^2-\varepsilon_d k_\omega^2)^{-1/2}$ from the crystal boundary. The latter term does not carry energy out of the junctions. In particular, for $k_z=0$, we have $B_y(L,0)=-\sqrt{\varepsilon_d}E_z(L,0)$, leading to the simple boundary condition for the homogeneous oscillating phase in the limit $L_y,L_z\gg\lambda_0$, $\nabla_x\theta_\omega=\pm(i\sqrt{\varepsilon_d}\omega/c)\theta_\omega$ for $x=L$ and 0. The relation (A6) can also be rewritten in the frequency-space representation as

$$B_y(L,z,\omega)=-\int_{-\infty}^{\infty}dz'\,U(z-z',\omega)E_z(L,z',\omega),$$

$$U(z,\omega)=-\frac{\varepsilon_d}{2}[|k_\omega|J_0(\sqrt{\varepsilon_d}|k_\omega z|)+ik_\omega N_0(\sqrt{\varepsilon_d}|k_\omega z|)], \quad \text{(A7)}$$

where $J_0(z)$ and $N_0(z)$ are the Bessel functions.

The same approach can be used in the realistic case of a crystal small along the $z$ axis, $L_z<\lambda_0$, if we know the radiated electric field at the planes $x=0$ and $L$ outside of the crystal, at $|z|>L_z/2$. If we put well conducting screens there, we can approximate $E_z=0$ at $|z|>L_z/2$. In this case for the homogeneous $n$-independent electric field, we obtain for the average magnetic field at the edge

$$\overline{B_y}(L,\omega)\approx-\frac{L_z\varepsilon_d}{2}\left[|k_\omega|-\frac{2i}{\pi}k_\omega\ln\frac{C}{\sqrt{\varepsilon_d}L_z|k_\omega|}\right]E_z(L,\omega), \quad \text{(A8)}$$

with $C=2\exp(3/2-\gamma_E)\approx5.03$, where $\gamma_E\approx0.5772$ is the Euler constant. We can see that for a small-size mesa, the magnetic field at the boundary is reduced by the factor $\sim L_z k_\omega$ in comparison to the infinite-$L_z$ case. This gives the following boundary condition for the oscillating phase:

$$\nabla_x\theta_\omega=\pm\frac{ik_\omega L_z\varepsilon_d}{2}\left[|k_\omega|-\frac{2i}{\pi}k_\omega\ln\frac{C}{\sqrt{\varepsilon_d}L_z|k_\omega|}\right]\theta_\omega \quad \text{(A9)}$$

for $x=L$ and 0. This corresponds to the boundary conditions (6) and (7) in reduced coordinates and $\varepsilon_d=1$ used in the paper. Therefore, for short crystals, the boundary condition cannot be written in the form of an instantaneous relation in between the space and time derivatives of the phase. This significantly complicates their numerical implementation. Screens also completely isolate semispaces $x>L$ and $x<0$, and eliminate interference of radiation coming from the opposite edges.

## APPENDIX B: RADIATED POWER FROM A RECTANGULAR MESA

The radiation power from a short rectangular mesa can be found approximately. For such a mesa, radiation influences weakly the shape of the resonance mode. In such a situation, the radiation is mostly determined by the distribution of the oscillating electric field at the mesa edge, which, in turn, is determined by the shape of the internal mode. Finding the radiation occurs to be a somewhat easier problem than finding general boundary conditions for the oscillating phase. An approximate expression for the radiated electric field far away from the crystal and, thus, the radiation power can be calculated using Huyghens' principle, as it is developed in the theory of antennas (see, e.g., Ref. 31). This approach has been applied to resonance modes in rectangular capacitors in Ref. 28. Such a consideration clearly shows the role of screens and crystal geometry in the formation of the radiation. Huyghens' principle in the formulation of Schelkunoff (equivalence principle) states that we can find fields outside of real sources (currents and charges) if we know equivalent sources placed on some boundary surface surrounding real sources. In particular, the equivalent magnetic current $\mathbf{M}_s$ is related to the tangential components of the electric field $\mathbf{E}$ on the surface as

$$\mathbf{M}_s=-\frac{c}{4\pi}\mathbf{n}\times\mathbf{E}, \quad \text{(B1)}$$

where $\mathbf{n}$ is the normal vector on the boundary surface.

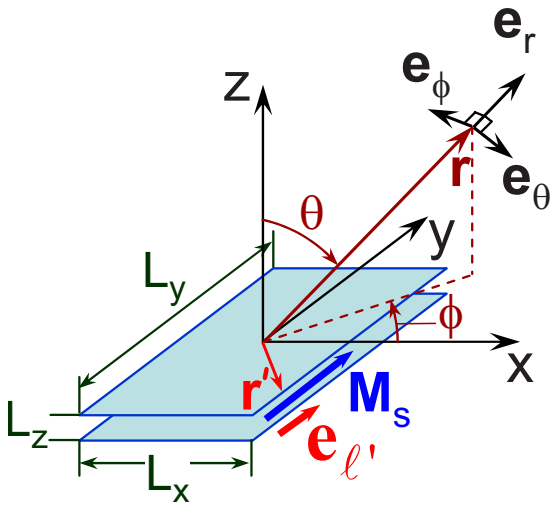


FIG. 8. (Color online) Geometry for radiation out of a rectangular mesa.

In the following, we consider the crystal inside the volume $0<x<L_x$, $0<y<L_y$, and $0<z<L_z$ bounded by thin metallic contacts on the top and bottom (see Fig. 8). The contacts are highly conductive, and there we can neglect the tangential electric field. At the crystal edges $x=0$ and $L_x$, we can neglect the magnetic field when the radiation power is small, as in the case of radiation from a capacitor with a small distance $L_z$ between electrodes, $k_\omega L_z \ll 1$ (see Ref. 28). In this case, we need to account only for the electric field at the crystal edges, which produces the magnetic equivalent currents (B1). They are related to the oscillating phases $\theta_\omega$ at these edges according to Eq. (A1). We consider modes inside the crystal which are uniform along the $z$ axis (synchronized Josephson oscillations in all intrinsic Josephson junctions). In this approximation, the electric field $E_z$ inside the crystal is described by standing waves characterized by the indices $m$ and $n$:

$$E_z(\mathbf{r}) = E_z(m,n)\cos(k_{x,m}x)\cos(k_{y,n}y),$$
$$k_{x,m} = \pi m/L_x, \quad k_{y,n} = \pi n/L_y. \tag{B2}$$

Faraway radiated electric field in terms of $E_z(n,m)$ is given by the expression

$$\mathbf{E} = -\frac{k_\omega L_z}{c}\frac{\exp(ik_\omega r)}{r}\int M_s(\mathbf{r}')\exp(-ik_\omega \mathbf{r}'\mathbf{e}_r)(\mathbf{e}_r \times \mathbf{e}_{\ell'})d\ell',$$

where the integral is taken over the perimeter of the crystal, and the coordinate system as well as definitions of the unit vectors $\mathbf{e}_r$ and $\mathbf{e}_{\ell'}$ are given in Fig. 8. Integration over contour $\ell$ gives the following result[28]:

$$\frac{\mathbf{E}}{E_z(m,n)} = \frac{L_z \exp(ik_\omega r)}{4\pi r}\left(\mathbf{P}_x \frac{k_\omega k_\xi}{k_{x,m}^2 - k_\xi^2} - \mathbf{P}_y \frac{k_\omega k_\eta}{k_{y,n}^2 - k_\eta^2}\right) G_x G_y,$$

where

$$\mathbf{P}_x = \sin\phi \mathbf{e}_\theta + \cos\theta\cos\phi \mathbf{e}_\phi,$$

$$\mathbf{P}_y = -\cos\phi \mathbf{e}_\theta + \cos\theta\sin\phi \mathbf{e}_\phi,$$

and

$$\begin{Bmatrix} k_\xi \\ k_\eta \end{Bmatrix} = k_\omega \sin\theta \begin{Bmatrix} \cos\phi \\ \sin\phi \end{Bmatrix}.$$

The interference factors $G_x = 1-(-1)^n \exp(ik_\xi L_x)$ and $G_y = 1-(-1)^m \exp(ik_\eta L_y)$ describe the contribution of waves coming to the faraway point $\mathbf{r}$ from opposite sides of the crystal $x'=0$ and $x'=L_x$ along the $x$ axis as well as from opposite sides $y'=0$ and $y'=L_y$, respectively. Their role in the formation of the radiation becomes clear if we will consider different modes. From the radiated electric field, we can compute the total radiated power as

$$P = \frac{c}{8\pi} r^2 \int_{-\pi}^{\pi} d\phi \int_0^{\pi} \sin\theta d\theta [|E_\theta|^2 + |E_\phi|^2]. \tag{B3}$$

For homogeneous oscillations $m=n=0$, we obtain

$$\frac{\mathbf{E}}{E_z(0,0)} = -\frac{L_z \exp(ik_\omega r)}{4\pi r}\left(\frac{k_\omega}{k_\xi}\mathbf{P}_x - \frac{k_\omega}{k_\eta}\mathbf{P}_y\right)[1-\exp(-ik_\xi L_x)] \times [1-\exp(-ik_\eta L_y)]$$

corresponding to

$$\frac{E_\theta}{E_z(0,0)} = -\frac{L_z \exp(ik_\omega r)}{4\pi r}\frac{[1-\exp(-ik_\omega L_x \sin\theta\cos\phi)][1-\exp(-ik_\omega L_y \sin\theta\sin\phi)]}{\sin\theta\cos\phi\sin\phi}, \tag{B4}$$

and $E_\phi = 0$. The radiated power (B3) is given by

$$P = \frac{c|E_z(0,0)|^2}{32\pi^3}\int_{-\pi}^{\pi} d\phi \int_0^{\pi} d\theta \frac{[1-\cos(k_\omega L_x \sin\theta\cos\phi)][1-\cos(k_\omega L_y \sin\theta\sin\phi)]}{\sin\theta\cos^2\phi\sin^2\phi}.$$

For small-size crystal $L_x, L_y \ll k_\omega^{-1}$ with almost uniform Josephson oscillations, we obtain

$$P = \frac{c|E_z(0,0)|^2}{48\pi^2} k_\omega^4 L_x^2 L_y^2 L_z^2. \tag{B5}$$

This is the result for dipole radiation because all sizes of the crystal are small in comparison with the wavelength of the radiated field. For the crystal with size $L_y$ bigger than the radiation wavelength, $k_\omega L_y \gg 1$, the result is quite different:

$$P \approx \frac{\omega L_y L_z^2 |E_z(0,0)|^2}{16\pi} [1 - J_0(k_\omega L_x)]. \tag{B6}$$

Now the waves coming from opposite sides of the crystal along the $y$ axis do not interfere with each other and radiation power becomes proportional to $L_y$. For $k_\omega L_x \ll 1$, we obtain the power proportional to $k_\omega^2 L_x^2$ due to destructive interference of the waves coming from opposite sides of the crystal along the $x$ axis. If we put highly conductive metallic screens separating the spaces $x > L_x$ and $x < 0$ so that the edge $x=0$ radiates only into $x<0$ half-space, while that at $x=L_x$ radiates only into $x>L_x$ half-space (see Fig. 2), the interference will be eliminated. Such screens also double the radiation coming from one side. This can be demonstrated in the simplest way using image technique:[31] radiation from the real electric currents induced at the screens is equivalent to radiation from the image magnetic current placed next to the original magnetic current. This leads to doubling of the effective magnetic current, $M_s \to 2M_s$, and quadruples the radiated power density. As the radiation now is limited only by half-space, the total radiated power doubles. Therefore, in the presence of screens, the factor $[1-J_0(k_\omega L_x)]$ in Eq. (B6) has to be replaced by the factor 2. This means that the screens strongly enhance the radiation induced by the homogeneous mode in the case $k_\omega L_x \ll 1$. Such a design with screens for a crystal thin along the $x$ axis was proposed in Ref. 23. This design gives the possibility of frequency tuning. In addition, heating is reduced due to small $L_x$. However, the crystal should have a large number of layers to synchronize oscillations in all junctions and work in the superradiation regime.

Next, we consider the fundamental cavity mode $(m,n)=(1,0)$, more relevant for the subject of this paper. In this case, we obtain

$$\frac{\mathbf{E}}{E_z(1,0)} = \frac{L_z \exp(ik_\omega r)}{4\pi r}\left(\mathbf{P}_x \frac{k_\omega k_\xi}{(\pi/L_x)^2 - k_\xi^2} + \mathbf{P}_y \frac{k_\omega}{k_\eta}\right) \times [1 - \exp(-ik_\xi L_x)][1 + \exp(-ik_\eta L_y)].$$

The components of the faraway electric field are given by the expressions

$$\frac{E_\theta}{E_z(1,0)} = -\frac{L_z \exp(ik_\omega r)}{4\pi r} \frac{\sin^2\theta - (\pi/a_x)^2}{\sin^2\theta\cos^2\phi - (\pi/a_x)^2} \frac{\cos\phi}{\sin\theta\sin\phi} \times [1 + \exp(-ia_x \sin\theta\cos\phi)] \times [1 - \exp(-ia_y \sin\theta\sin\phi)],$$

$$\frac{E_\phi}{E_z(1,0)} = -\frac{L_z \exp(ik_\omega r)}{4\pi r} \frac{(\pi/a_x)^2}{\sin^2\theta\cos^2\phi - (\pi/a_x)^2} \frac{\cos\theta}{\sin\theta} \times [1 + \exp(-ia_x \sin\theta\cos\phi)] \times [1 - \exp(-ia_y \sin\theta\sin\phi)],$$

with $a_x = k_\omega L_x$ and $a_y = k_\omega L_y$. The radiated power (B3) can be represented as

$$P = \frac{cL_z^2 |E_z(1,0)|^2}{4\pi^3} \mathcal{I}_{1,0}(k_\omega L_x, k_\omega L_y), \tag{B7}$$

with

$$\mathcal{I}_{1,0}(a_x,a_y) = \int_0^{\pi/2} d\phi \int_0^{\pi/2} d\theta \frac{[1+\cos(a_x \sin\theta\cos\phi)][1-\cos(a_y\sin\theta\sin\phi)]}{\sin\theta\sin^2\phi} \frac{[\sin^2\theta - (\pi/a_x)^2]^2\cos^2\phi + (\pi/a_x)^4\cos^2\theta\sin^2\phi}{[\sin^2\theta\cos^2\phi - (\pi/a_x)^2]^2}. \tag{B8}$$

In the regime $k_\omega L_y \gg 1$, this gives the following result:

$$P \approx \frac{\omega L_y L_z^2 |E_z(1,0)|^2}{16\pi} [1 + J_0(k_\omega L_x)]. \tag{B9}$$

Now we have a constructive interference of waves coming from opposite sides of the crystal along the $x$ axis because electric field on these sides has opposite signs generating the same-sign magnetic fields. For such mode, screens do not influence much the radiation in the limit $k_\omega L_x \ll 1$. The reduced parameter of radiation damping $\nu_r$ introduced in Eqs. (20) and (21) is related to the radiation power as

$$P = \nu_r L_x L_y L_z \frac{\varepsilon_c \omega_p}{16\pi} |E_z(1,0)|^2. \tag{B10}$$

The above results can also be straightforwardly generalized to the case when a stack is bounded by large-size ground plate at the bottom, $z=0$, see Fig. 2 (right). This is the case, for example, for the mesa fabricated on the top of bulk crystal. If we treat the ground plate as an ideal conductor, its influence can again be taken into account by the image technique.[31] This just leads to the doubling of the effective magnetic current, $\mathbf{M}_s \to 2\mathbf{M}_s$, and to the doubling of the total radiated power $P \to 2P$.

[1] B. D. Josephson, Phys. Lett. **1**, 251 (1962).
[2] I. K. Yanson, V. M. Svistunov, and I. M. Dmitrenko, Zh. Eksp. Teor. Fiz. **48**, 976 (1965); [Sov. Phys. JETP **21**, 650 (1965)]; I. K. Yanson, Low Temp. Phys. **30**, 516 (2004).
[3] D. N. Langenberg, D. J. Scalapino, B. N. Taylor, and R. E. Rice, Phys. Rev. Lett. **15**, 294 (1965).
[4] A. K. Jain, K. K. Likharev, J. E. Lukens, and J. E. Sauvageau, Phys. Rep. **109**, 309 (1984).
[5] M. Darula, T. Doderer, and S. Beuven, Supercond. Sci. Technol. **12**, R1 (1999).
[6] P. Barbara, A. B. Cawthorne, S. V. Shitov, and C. J. Lobb, Phys. Rev. Lett. **82**, 1963 (1999); B. Vasilić, S. V. Shitov, C. J. Lobb, and P. Barbara, Appl. Phys. Lett. **78**, 1137 (2001); B. Vasilić, P. Barbara, S. V. Shitov, and C. J. Lobb, Phys. Rev. B **65**, 180503(R) (2002).
[7] W. A. Al-Saidi and D. Stroud, Phys. Rev. B **65**, 224512 (2002); E. Almaas and D. Stroud, *ibid.* **63**, 144522 (2001); **65**, 134502 (2002); **67**, 064511 (2003).
[8] G. Filatrella, N. F. Pedersen, and K. Wiesenfeld, Phys. Rev. E **61**, 2513 (2000); G. Filatrella, N. F. Pedersen, C. J. Lobb, and P. Barbara, Eur. Phys. J. B **34**, 3 (2003).
[9] R. Kleiner, F. Steinmeyer, G. Kunkel, and P. Müller, Phys. Rev. Lett. **68**, 2394 (1992); R. Kleiner and P. Müller, Phys. Rev. B **49**, 1327 (1994).
[10] Yu. I. Latyshev, J. E. Nevelskaya, and P. Monceau, Phys. Rev. Lett. **77**, 932 (1996).
[11] O. K. C. Tsui, N. P. Ong, Y. Matsuda, Y. F. Yan, and J. B. Peterson, Phys. Rev. Lett. **73**, 724 (1994); O. K. C. Tsui, N. P. Ong, and J. B. Peterson, Phys. Rev. Lett. **76**, 819 (1996).
[12] Y. Matsuda, M. B. Gaifullin, K. Kumagai, K. Kadowaki, and T. Mochiku, Phys. Rev. Lett. **75**, 4512 (1995); Y. Matsuda, M. B. Gaifullin, K. I. Kumagai, M. Kosugi, and K. Hirata, *ibid.* **78**, 1972 (1997).
[13] H. B. Wang, P. H. Wu, and T. Yamashita, Phys. Rev. Lett. **87**, 107002 (2001).
[14] Yu. I. Latyshev, M. B. Gaifullin, T. Yamashita, M. Machida, and Y. Matsuda, Phys. Rev. Lett. **87**, 247007 (2001).
[15] A. Irie, Y. Hirai, and G. Oya, Appl. Phys. Lett. **72**, 2159 (1998).
[16] V. M. Krasnov, N. Mros, A. Yurgens, and D. Winkler, Phys. Rev. B **59**, 8463 (1999).
[17] S.-M. Kim, H. B. Wang, T. Hatano, S. Urayama, S. Kawakami, M. Nagao, Y. Takano, T. Yamashita, and K. Lee, Phys. Rev. B **72**, 140504(R) (2005).
[18] R. Kleiner, Phys. Rev. B **50**, 6919 (1994).
[19] L. N. Bulaevskii and A. E. Koshelev, J. Supercond. Novel Magn. **19**, 349 (2006).
[20] I. Kakeya, M. Iwase, T. Yamamoto, and K. Kadowaki, Proceedings of the FIM/ITS-NS/CTC/PLASMA 2004, Tsukuba, 24–28 November 2004, arXiv:cond-mat/0503498 (unpublished).
[21] A. E. Koshelev, Physica C **437-438**, 157 (2006); Phys. Rev. B **75**, 214513 (2007).
[22] M. Tachiki, M. Iizuka, K. Minami, S. Tejima, and H. Nakamura, Phys. Rev. B **71**, 134515 (2005).
[23] L. N. Bulaevskii and A. E. Koshelev, Phys. Rev. Lett. **99**, 057002 (2007).
[24] M. Russo and R. Vaglio, Phys. Rev. B **17**, 2171 (1978).
[25] L. Ozyuzer, A. E. Koshelev, C. Kurter, N. Gopalsami, Q. Li, M. Tachiki, K. Kadowaki, T. Yamamoto, H. Minami, H. Yamaguchi, T. Tachiki, K. E. Gray, W.-K. Kwok, and U. Welp, Science **318**, 1291 (2007).
[26] Throughout the paper, in estimates we use parameters typical for moderately underdoped BSCCO at low temperatures. Usage of the underdoped BSCCO in the discussed design is preferable for reducing heating due to smaller quasiparticle conductivity.
[27] Note that, in general, the radiation damping parameter $\nu_r$ depends not only on stack geometry but also on the excited mode. Only in the case considered here ($k_\omega L_y \gg 1$ and no interference between radiation from the opposite edges), $\nu_r$ is the same for all $m$.
[28] M. Leone, IEEE Trans. Electromagn. Compat. **45**, 486 (2003).
[29] G. Yang, J. S. Abell, and C. E. Gough, Appl. Phys. Lett. **75**, 1955 (1999).
[30] V. M. Krasnov, A. Yurgens, D. Winkler, and P. Delsing, J. Appl. Phys. **89**, 5578 (2001); J. C. Fenton and C. E. Gough, *ibid.* **94**, 4665 (2003); V. N. Zavaritsky, Phys. Rev. B **72**, 094503 (2005); V. M. Krasnov, M. Sandberg, and I. Zogaj, Phys. Rev. Lett. **94**, 077003 (2005); H. B. Wang, T. Hatano, T. Yamashita, P. H. Wu, and P. Muller, Appl. Phys. Lett. **86**, 023504 (2005); Myung-Ho Bae, Jae-Hyun Choi, and Hu-Jong Lee, *ibid.* **86**, 232502 (2005); X. B. Zhu, Y. F. Wei, S. P. Zhao, G. H. Chen, H. F. Yang, A. Z. Jin, and C. Z. Gu, Phys. Rev. B **73**, 224501 (2006).
[31] R. S. Elliott, *Antenna Theory and Design* (IEEE/Wiley Interscience, Hoboken, New Jersey, 2003).